

Role of Second Halogen Atoms of Dihalobenzene in Controlling the Photoluminescence Properties of Single-Walled Carbon Nanotubes by Reductive Arylation

Yutaka Maeda,* Atsushi Suwa, Kentaro Kawada, Pei Zhao, Masahiro Ehara,* Yasuhiro Suzuki, Yui Iguchi, Yasunari Taki, Yui Konno, Michio Yamada, Hitoshi Kasai, Koji Kimoto, and Koji Harano*



Cite This: *ACS Nanosci. Au* 2026, 6, 270–280



Read Online

ACCESS |



Metrics & More



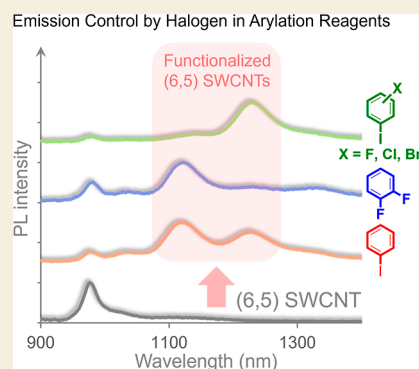
Article Recommendations



Supporting Information

ABSTRACT: The chemical functionalization of single-walled carbon nanotubes (SWCNTs) is effective for controlling their near-infrared (NIR) photoluminescence (PL) wavelength by locally modulating the band gap energy of the SWCNTs. The PL efficiency is dependent on the degree of functionalization. Herein, SWCNTs were reductively arylated using sodium naphthalenide and halo- and dihalobenzene derivatives to control their PL properties. (6,5) SWCNTs functionalized with iodobenzene exhibited two new PL peaks at 1100 and 1230 nm. In contrast, the arylated SWCNTs prepared by using fluorobenzene and chlorobenzene exhibited a single new PL peak at 1100 nm. Furthermore, the arylated SWCNTs prepared using dihalobenzene derivatives except for 1,2-difluorobenzene exhibited a new PL peak at 1230 nm, which was dependent on the type and number of halogen atoms. The relative stabilities and transition energies of the model compounds for the arylated SWCNTs were estimated by using theoretical calculations. These results suggest that their transition energies can be tuned by the binding configuration and that the relative stability of the binding configuration varies depending on the addenda. The arylated SWCNTs were chirally separated, and an analysis of the optical properties of the separated SWCNT adducts revealed that this arylation reaction is effective for tuning the PL wavelength and intensity of (6,4), (7,3), (8,3), and (7,5) SWCNTs with different chiral indices in the NIR region. The addenda on the SWCNTs were successfully observed using transmittance electron microscopy by isolating the functionalized (6,5) SWCNTs and subsequent thermal treatment.

KEYWORDS: single-walled carbon nanotubes, infrared, photoluminescence, functionalization, transmission electron microscopy



INTRODUCTION

The chemical functionalization of single-walled carbon nanotubes (SWCNTs) has been investigated to elucidate their chemical reactivity and introduce functions.^{1–4} The SWCNT structure varies with the diameter and chiral angle and is distinguished by its chiral index, which is defined by a vector on the graphene lattice.⁵ The functionalization of semi-conducting SWCNTs is expected to be a method to generate new near-infrared (NIR) photoluminescence (PL) peaks in a longer wavelength region, as compared with pristine SWCNTs.^{6–13} Theoretical studies indicated that functionalization decreases the local band gap of SWCNTs, with the amount of change being dependent on the binding configuration of the addenda.^{13–17} An early study on the arylation of SWCNTs using aryl diazonium salts demonstrated the emergence of a new PL peak at 1119 nm from phenylated (6,5) SWCNTs.¹³ Interestingly, the PL wavelength can be tuned by the substituent effect of the phenyl groups. For example, the PL peaks resulting from functionalization with 4-nitro and 4-(*N,N*-diethylamino)benzenediazonium salts were observed at 1137 and 1110 nm, respectively, owing to

electronic effects, showing good correlation with the Hammett substituent constants. Wang et al. reported that the functionalization of (6,5) SWCNTs using 2-sulfonylbenzenediazonium salt and alcohol exhibits new PL peaks at 1240–1270 nm, depending on the steric effects of reagents.¹⁸ Yu et al. reported that the functionalization of (6,5) SWCNTs using 2-ethynyl or 2-phenylbenzenediazonium salts exhibits new PL peaks at 1230–1263 nm, which was attributed to the π – π interaction between the SWCNTs and the π -conjugated substituents.¹⁹ Maeda et al. reported the arylation reaction of (6,5) SWCNTs using sodium naphthalenide and iodobenzene derivatives, which resulted in the emergence of two new PL peaks at 1100 and 1230 nm. Using 4-methoxyiodobenzene and 2-methoxyiodobenzene instead of iodobenzene improved the

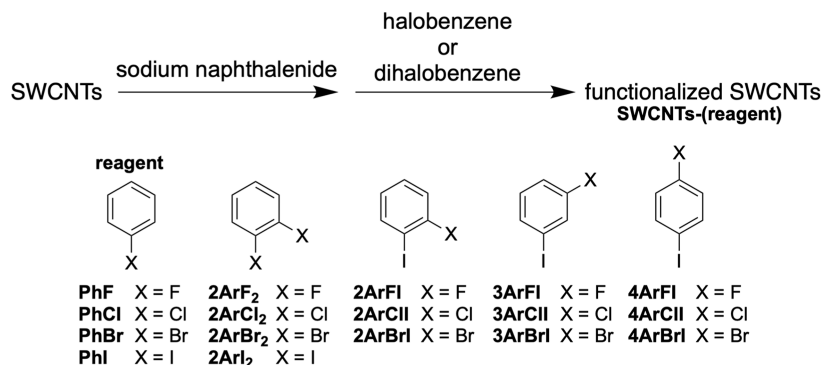
Received: October 6, 2025

Revised: December 19, 2025

Accepted: December 19, 2025

Published: December 29, 2025



Scheme 1. Functionalization of SWCNTs Using Halobenzene (PhX) and Dihalobenzene Derivatives (nArX₂)^a

^aThe amounts of reagents used in the reaction per 1 mg of SWCNTs unless otherwise stated: PhX, 0.281 mmol. nArX₂, 0.141 mmol. Sodium naphthalenide, 0.234 mmol.

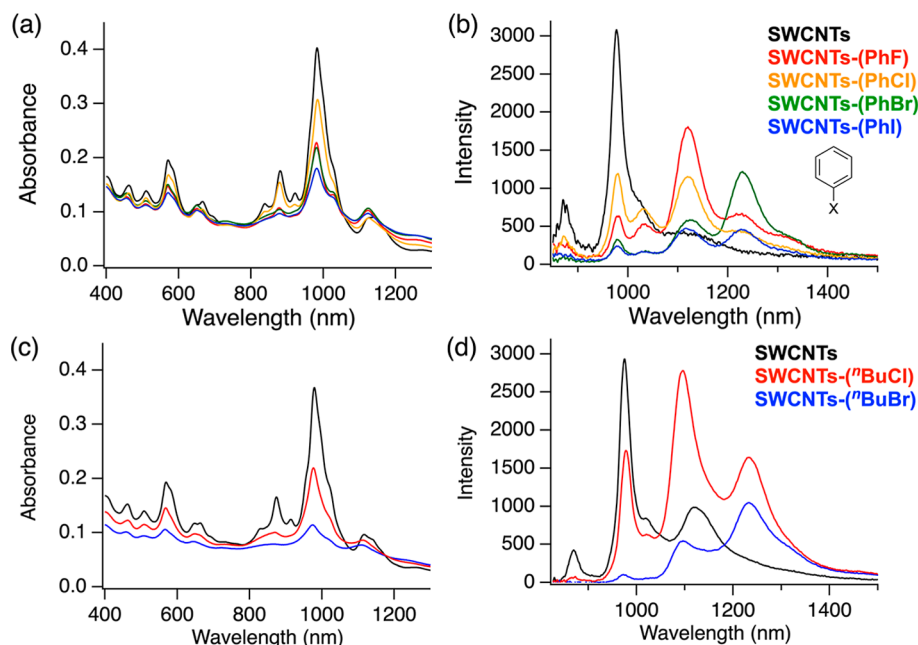


Figure 1. (a, c) Absorption and (b, d) PL spectra of SWCNTs (black) and functionalized SWCNTs. (b) SWCNTs-(PhX) (red: X = F (Ex: 568 nm), yellow: X = Cl (Ex: 566 nm), green: X = Br (Ex: 568 nm), blue: X = I (Ex: 567 nm)). (d) SWCNTs-(ⁿBuX) (red: X = Cl (Ex: 567 nm), blue: X = Br (Ex: 567 nm)).

Table 1. PL Wavelength (nm) of Functionalized SWCNTs

	PL wavelength			PL wavelength
	E ₁₁ * PL	E ₁₁ ** PL		E ₁₁ ** PL
SWCNTs-(PhF)	1121	1228	SWCNTs-(2ArFI)	1227
SWCNTs-(PhCl)	1119		SWCNTs-(2ArClI)	1230
SWCNTs-(PhBr)	1124	1230	SWCNTs-(2ArBrI)	1230
SWCNTs-(PhI)	1116	1227	SWCNTs-(3ArFI)	1231
SWCNTs-(2ArF ₂)	1122		SWCNTs-(3ArClI)	1230
SWCNTs-(2ArCl ₂)	1122	1227	SWCNTs-(3ArBrI)	1230
SWCNTs-(2ArBr ₂)		1230	SWCNTs-(4ArFI)	1230
SWCNTs-(2ArI ₂)		1230	SWCNTs-(4ArClI)	1228
			SWCNTs-(4ArBrI)	1228

selectivity of the PL peaks at 1100 and 1230 nm in (6,5) SWCNTs, respectively, with the change in their functionalization degree, owing to the steric effect of the reactants.²⁰ Maeda et al. reported another method for controlling the PL wavelength using alkyl lithium reagents as a factor of steric

hindrance.^{21,22} Each method attempts to control the PL wavelength by changing the binding configuration. Depending on the reactivity and substitution position, the halogen atoms on the benzene ring are expected to act as reactive sites or exert steric or electronic effects as substituents.²³ In this study,

Scheme 2. Plausible Reaction Mechanism and Products of the Reductive Arylation of SWCNTs Using PhX

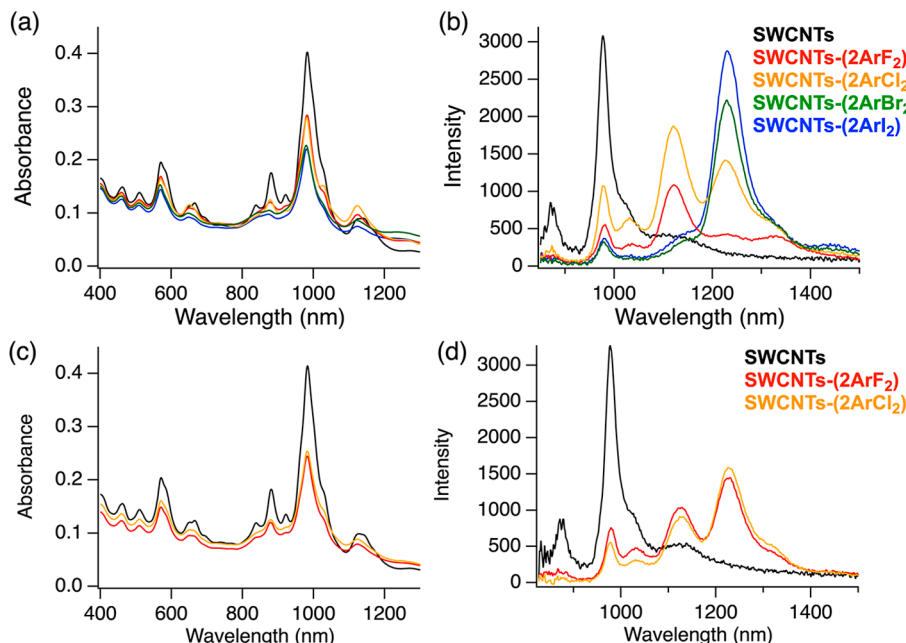
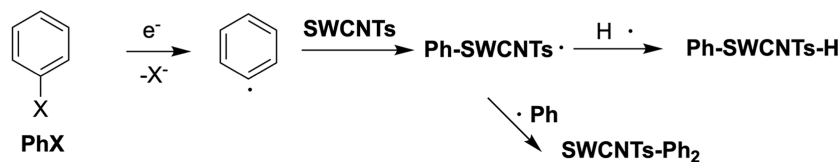


Figure 2. (a, c) Absorption and (b, d) PL spectra of SWCNTs (black) and functionalized SWCNTs. (a, b) Reagents ratio 2ArX_2 :sodium naphthalenide = 0.6:1. Red: X = F (Ex: 566 nm), yellow: X = Cl (Ex: 568 nm), green: X = Br (Ex: 569 nm), and blue: X = I (Ex: 568 nm). (c, d) Reagents ratio 2ArX_2 :sodium naphthalenide = 1.2:1. Red: X = F (Ex: 570 nm) and yellow: X = Cl (Ex: 570 nm).

SWCNTs were functionalized using various halobenzene and dihalobenzene derivatives, shown in Scheme 1, to study the effects of halogen atoms on the degree of functionalization and PL properties of functionalized SWCNTs.

RESULTS AND DISCUSSION

Figures 1, S1, and S2 show the absorption, PL, and Raman spectra of SWCNTs-(PhX) and SWCNTs-(ⁿBuX). The changes in the E_{11} absorption and E_{11} PL peak intensities and the relative intensity of the D band compared to the G band (D/G) indicated the degree of functionalization of the SWCNT adducts. The spectral changes and D/G suggested that the degrees of functionalization of SWCNT-(PhF) and SWCNT-(PhCl) were relatively lower than those of SWCNT-(PhBr) and SWCNT-(PhI). The reduction potential of halobenzene is reportedly PhCl: -2.78 , PhBr: -2.44 , and PhI: -2.24 V vs SCE. The functionalization degree of the SWCNT adducts showed good agreement with the reduction potential of halobenzenes.²⁴ SWCNTs-(PhF) and SWCNTs-(PhCl), which exhibit a lower functionalization degree, mainly emerged as new PL peaks at approximately 1120 nm (E_{11}^* PL). In contrast, SWCNTs-(PhBr) exhibited a high PL peak selectivity at approximately 1230 nm (E_{11}^{**} PL). Table 1 lists the PL wavelengths of the functionalized SWCNTs.

To investigate the relationship between the degree of functionalization and the selectivity of E_{11}^* and E_{11}^{**} PL, SWCNTs were reacted with a butyl halide (ⁿBuX, where X = Cl and Br). The E_{11} absorption and E_{11} PL peak intensities of

the butylated SWCNTs (SWCNTs-(ⁿBuCl) and SWCNTs-(ⁿBuBr)) indicate that a higher degree of functionalization can be achieved using ⁿBuBr than using ⁿBuCl. Regarding the selectivity of the PL wavelength, similar to the case for the halobenzene system, the intensity ratio of E_{11}^{**} PL to E_{11}^* PL increased with an increasing functionalization degree.²⁵ As mentioned in the Introduction section, the hydrobutylation and dibutylation reactions of (6,5) SWCNTs reportedly afford E_{11}^* and E_{11}^{**} PL peaks, respectively, and the 1,2- and 1,4-addition products are thermodynamically preferred products for hydrobutylated and dibutylated SWCNTs, respectively. A possibility exists that hydrophenylation and diphenylation occur in the reaction with halobenzene, with the latter expected to occur preferentially with an increasing halobenzene reactivity (Scheme 2).

Figures 2, S1, and S2 depict the Raman, absorption, and PL spectra of SWCNTs-(2ArX_2). SWCNTs-(2ArBr_2) and -(2ArI_2), which exhibited higher degrees of functionalization than SWCNTs-(2ArF_2) and -(2ArCl_2), selectively exhibited E_{11}^{**} PL. SWCNTs-(2ArCl_2) exhibited E_{11}^* and E_{11}^{**} PL peaks, regardless of the amount of 2ArCl_2 used. The E_{11}^* and E_{11}^{**} PL peaks were observed for SWCNTs-(2ArF_2) (Figure 2d, reagent ratio used: 2ArF_2 :sodium naphthalenide = 1.2:1). However, SWCNTs-(2ArF_2) (Figure 2b, reagent ratio used: 2ArF_2 :sodium naphthalenide = 0.6:1) selectively exhibited the E_{11}^* PL peak. These results suggest that the type of halogen atom and amount of 2ArX_2 used for the reductant are important factors for the selective emergence of a new PL

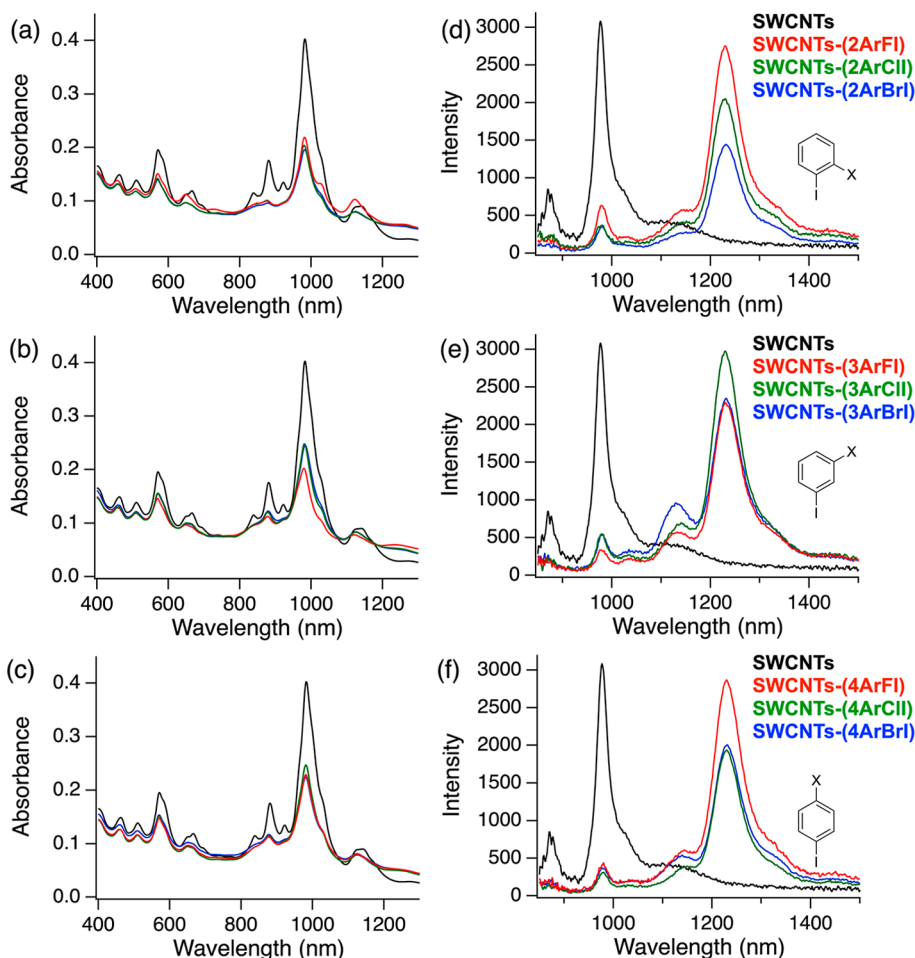
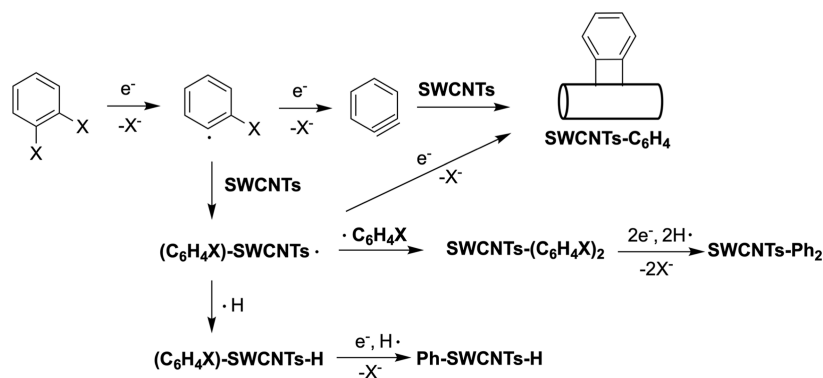
Scheme 3. Plausible Reaction Mechanism of the Reductive Arylation of SWCNTs Using 2ArX₂ (X = F, Cl, Br, I)

Figure 3. (a–c) Absorption and (d–f) PL spectra of SWCNTs-(*n*ArXI). Red: X = F. Green: X = Cl. Blue: X = Br. (Ex: 566 nm for SWCNTs-(3ArXI) and -(4ArXI); Ex: 567 nm for SWCNTs-(2ArBrI); Ex: 568 nm for SWCNTs-(2ArFI) and -(2ArClI)).

peak. The generation efficiency of aryl radicals affects the production efficiency of hydroarylated and diarylated SWCNT derivatives. In contrast, it is possible that the reaction with 1,2-dihaloaromatic derivatives can lead to a cycloaddition adduct (SWCNTs-C₆H₄) via stepwise radical addition or aryne formation (Scheme 3).^{26,27}

The reaction of SWCNTs using 2-substituted iodobenzene derivatives (2ArXI, X = F, Cl, Br) was conducted. As shown in Figure 3, each functionalized SWCNT (SWCNTs-(2ArXI)) selectively exhibited the E₁₁** PL peak. Interestingly, the E₁₁** PL peak also selectively appeared in reactions with

3ArXI and 4ArXI, which are not considered suitable for the formation of cycloaddition products. In addition, similar E₁₁ absorption and E₁₁ PL peak intensities were observed in SWCNTs-(2-ArXI), -(3ArXI), and -(4ArXI). This result indicated that the influence of the second halogen atom of *n*ArXI on the degree of functionalization is weak in this reaction system. In the X-ray photoelectron spectroscopy (XPS) measurements, a lower atomic percentage of halogen atoms was observed in SWCNTs-(*n*ArXI) (*n* = 2, 3, 4; X = F and Cl), as compared to SWCNTs-(*n*ArBrI) (*n* = 2, 3, 4), indicating that the Cl and F atoms tend to remain in the

phenyl group more than the Br and I atoms (Table 2, Figures S3–S5). A plausible explanation is that reagents bearing two

Table 2. Atomic Percentage of SWCNTs-(nXI)

	C	F	I
SWCNTs-(2ArFI)	94.9	5.0	0.1
SWCNTs-(3ArFI)	99.5	0.4	0.1
SWCNTs-(4ArFI)	97	2.9	0.1
	C	Cl	I
SWCNTs-(2ArClI)	99.8	0.1	0.1
SWCNTs-(3ArClI)	99.8	0.2	0.1
SWCNTs-(4ArClI)	99.7	0.2	0.1
	C	Br	I
SWCNTs-(2ArBrI)	99.9	0.0	0.1
SWCNTs-(3ArBrI)	99.8	0.1	0.1
SWCNTs-(4ArBrI)	99.8	0.1	0.1

highly reactive halogen atoms (nArBrI: $n = 3, 4$) increase the generation efficiency of radical intermediates, thereby promoting the formation of 1,4-diarylated SWCNTs (Scheme 4). Even if the generated radical species do not participate in bonding with SWCNTs, they are expected to capture the hydrogen atom, thereby suppressing the formation of 1,2-hydroarylated SWCNTs (Ar-SWCNTs-H and/or Ph-SWCNTs-H).

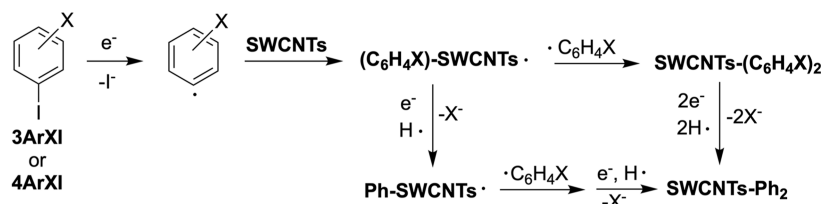
The chiral separation^{28,29} of SWCNTs-(nArFI) ($n = 2, 3, 4$), selectively exhibiting E_{11}^{**} PL with a relatively high PL efficiency for (6,5) SWCNTs, was conducted to confirm the effect of functionalization on the other chiral SWCNTs. Figures 4 and S7–S12 show the Raman, absorption, and PL spectra of the separated SWCNT derivatives. The PL peaks were assigned to the absorption and excitation wavelengths. Both the E_{11}^* PL and E_{11}^{**} PL peaks emerged in (6,4) SWCNTs-(3ArFI) and (6,4) SWCNTs-(4ArFI). In contrast, the other (n,m) SWCNTs-(nArFI) selectively exhibited E_{11}^{**} PL. As shown in Table 3, the introduced fluorine atom is effective at improving the PL wavelength selectivity. For all SWCNTs except for (7,3) SWCNTs, there is no significant difference in the E_{11}^{**} PL wavelength as compared to SWCNTs-(PhI). The separated SWCNTs-(3ArFI) and -(4ArFI) exhibited relatively high D/G values compared with those of SWCNTs-(PhI) and -(2ArFI) (Figure S9, Table S2). However, due to differences in purity between the fractions, the effects of the reagents on the functionalization degree of SWCNTs require further investigation.

The impact of the fluorine atom in the phenyl group of the diarylated SWCNTs on the relative stability and transition energy was evaluated using theoretical calculations.^{14–17,30–35} Tables S3–S7 list the transition and relative energies for hydrophenylated and diphenylated (6,5) SWCNTs and those of the fluorine-substituted derivatives. The six binding configurations of the two carbon atoms in the same hexagonal

ring on the SWCNTs were classified according to their orientations with respect to the SWCNT axis, which are denoted as L_{++} , L_{+-} , and L_{--} (Figure 5).¹⁷ The theoretical results showed a tendency for a slight decrease in the transition energy by replacing the hydrogen atom in the phenyl ring with a fluorine atom (Tables S4, S5, and S7). The similar PL wavelengths experimentally observed in (6,5) SWCNTs-(PhI) and (6,5) SWCNTs-(nArFI) support elimination of the fluorine atom. A similar effect of the fluorine atom on the transition energies of (7,3) SWCNT-(3-fluorophenyl)₂ and (8,3) SWCNT-(3-fluorophenyl)₂ was observed (Figure 5, Tables S8–S11). The PL peaks of (6,4) SWCNTs-(3ArFI), (6,4) SWCNTs-(4ArFI), (7,3) SWCNTs-(nArFI), and (8,3) SWCNTs-(3ArFI) were observed at wavelengths longer than those of SWCNTs-(PhI), suggesting that the fluorine atoms were not completely eliminated, which is in agreement with the XPS results.

Kwon et al.²⁶ and Gifford et al.²⁷ reported that the 1,2-cycloadducts of (6,5) SWCNTs prepared with 1,2-diiodobenzene exhibited a new PL peak at a longer wavelength (1162 nm) than that of the corresponding noncycloadducts prepared with iodobenzene (1129 nm). To confirm the formation of the cycloadducts SWCNT-C₆H₄ in the reductive arylation using nArX₂, theoretical calculations of the corresponding model compounds were performed to estimate the transition energies and thermodynamic stabilities of the isomers with different binding configurations. As shown in Table S12, 1,2 L_{++} was the most stable binding configuration for (6,5) SWCNT-C₆H₄, and its transition energy was closer to that of 1,2 L-Ph-(6,5) SWCNT-H (Table S6) than that of 1,4 L_{++} (6,5) SWCNT-Ph₂ (Table S3). In stepwise addition reactions, the spin density of the intermediate radical is an important factor from the kinetic control perspective.^{19,25,36,37} Whether the substituents are phenyl or alkyl groups, the 1,2 L_{++} and 1,2 L_{--} carbon atoms of the monofunctionalized SWCNT radicals have higher spin densities than the other 1,2- and 1,4-carbon atoms; thus, these carbon atoms are expected to be candidates for addition sites for the kinetic product (Table S14). Structure optimization was performed for the 1,3- and 1,4-cycloaddition of C₆H₄ to (6,5) SWCNT at the 1,2 L_{++} binding configuration; however, the relative energy of the 1,4-cycloaddition adduct was 99.9 kcal/mol higher relative to the most stable cycloaddition product, 1,2 L_{++} (6,5) SWCNT-C₆H₄ (1,2-cycloaddition), and no stable structure was obtained for the 1,3-cycloaddition. The transition energy of 1,2 L_{++} (6,5) SWCNT-C₆H₄ was high and close to those of 1,2 L_{--} (6,5) SWCNT-C₆H₄ and 1,2 L_{--} Ph-(6,5) SWCNT-H. Therefore, 1,4 L_{++} (6,5) SWCNT-Ph₂, rather than (6,5) SWCNT-C₆H₄, can be considered a plausible candidate for the 1230 nm emission. In the proposed model, the second halogen atom generates an aryl radical that traps a hydrogen atom to suppress hydroarylation, thereby promoting diarylation (Scheme 5). Hydrogen atom subtraction in this

Scheme 4. Plausible Reaction Mechanism of the Reductive Arylation of SWCNTs Using 3ArXI and 4ArXI (X = F, Cl, Br)



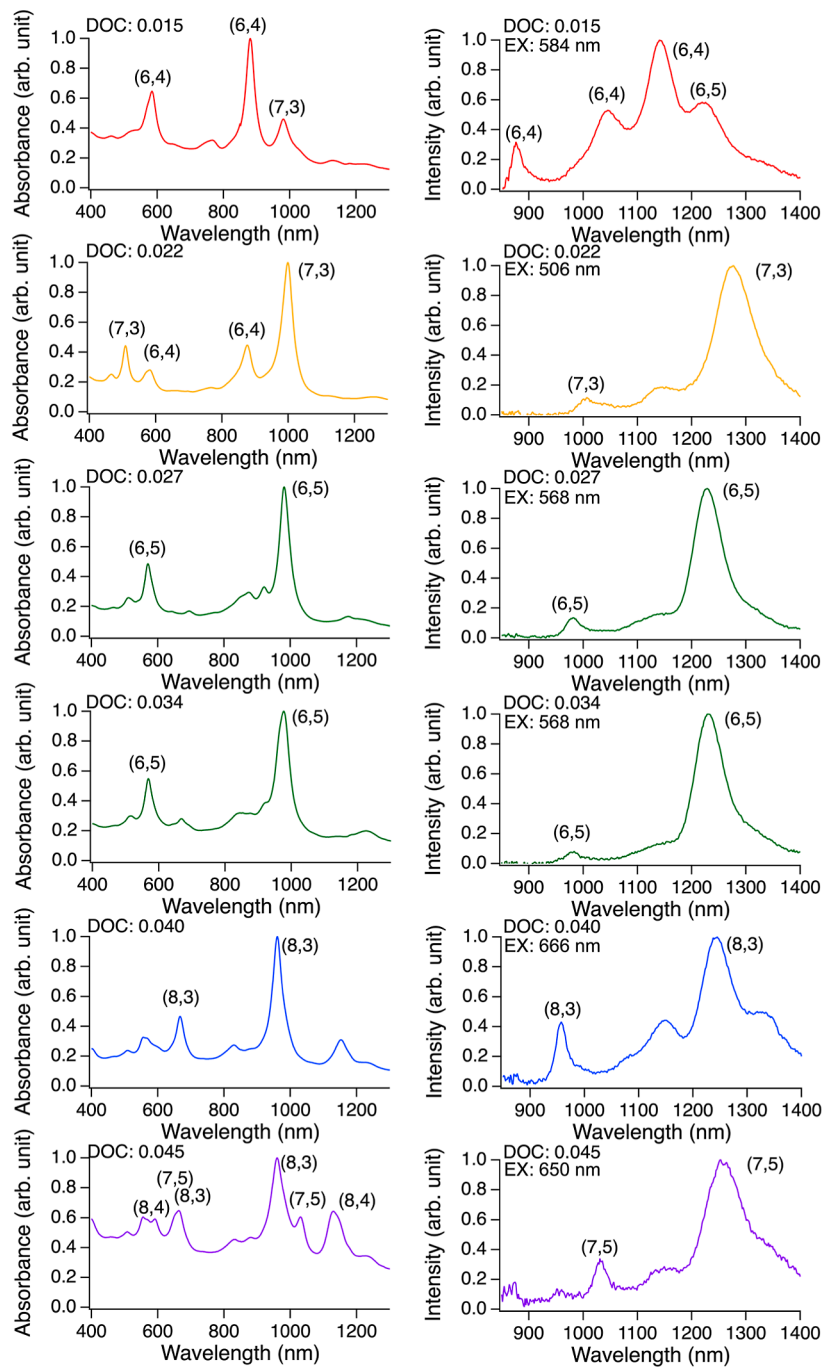


Figure 4. Absorption (left) and PL spectra (right) of separated SWCNTs-(4ArFI).

Table 3. PL Wavelength (nm) of the Separated SWCNTs and SWCNTs-(nArFI)

	(6,4)	(7,3)	(6,5)	(8,3)	(7,5)
SWCNTs	873	992	976	952	1024
SWCNTs-(PhI)	1043, 1137	1146,1262	1119,1228	1131,1237	1175,1264
SWCNTs-(2ArFI)	1140	1281	1229	1238	1264
SWCNTs-(3ArFI)	1048, 1141	1287	1231	1246	
SWCNTs-(4ArFI)	1047 1140	1269	1229	1238	1261

reaction was not identified, but THF is one possible source of hydrogen atoms.^{38,39}

Transmission electron microscopy (TEM) is an effective direct observation method that is widely applied to verify the structure of SWCNTs,^{1,2} the materials inside SWCNTs,⁴⁰ and

the addenda of functionalized SWCNTs.⁴¹ For TEM observation, chiral separation was conducted to remove impurities to obtain highly pure (6,5) SWCNTs-(2ArI₂) (Figure S14). Because a large amount of surfactant is required to disperse and separate SWCNTs, which interferes with the

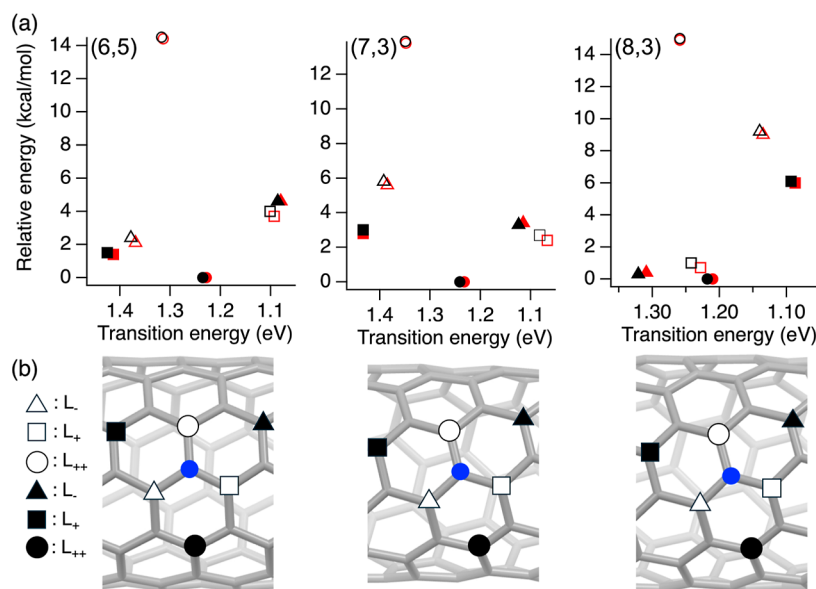


Figure 5. (a) Calculated transition and relative energies of model compounds for the diphenylated SWCNTs (black) and those of the fluorine-substituted derivatives (red) ((6,5) SWCNT-(4-fluorophenyl)₂, (7,3) SWCNT-(3-fluorophenyl)₂, and (8,3) SWCNT-(3-fluorophenyl)₂). (b) Six 1,2- and 1,4-binding configurations of (6,5), (7,3), and (8,3) SWCNTs relative to the first addition carbon atom (blue circle). \triangle : 1,2 L₋. \square : 1,2 L₊. \circ : 1,2 L₊₊. \blacktriangle : 1,4 L₋. \blacksquare : 1,4 L₊. \bullet : 1,4 L₊₊.

Scheme 5. One of the Plausible Models for Switching the PL Wavelength through the Use of an Additional Second Halogen Atom

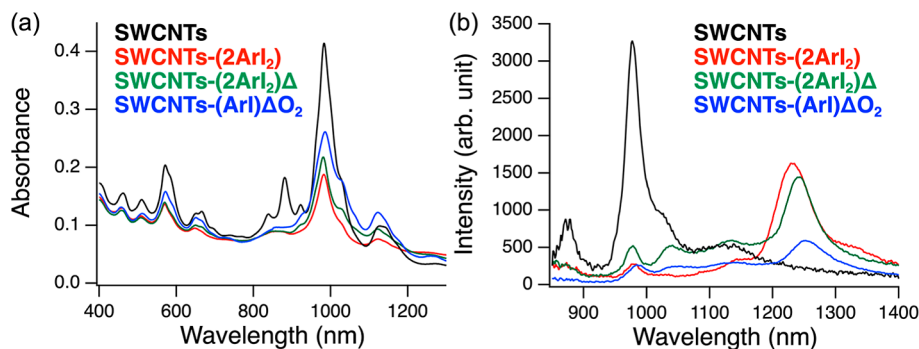
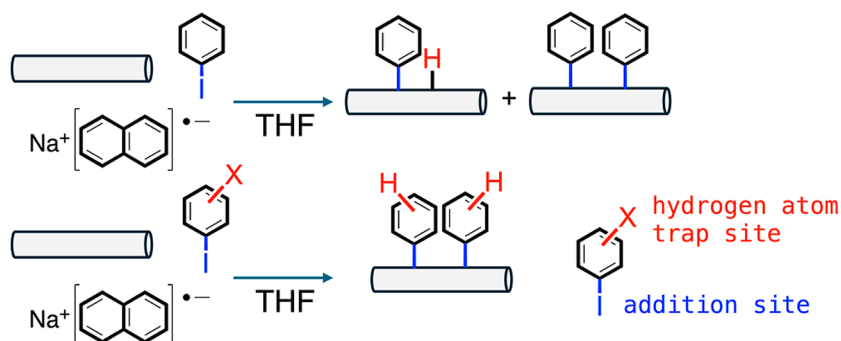


Figure 6. (a) Absorption and (b) PL spectra of SWCNTs (black), SWCNTs-(2ArI₂) (red, Ex: 570 nm), SWCNTs-(2ArI₂)Δ (green, Ex: 570 nm), and SWCNTs-(ArI)ΔO₂ (blue, Ex: 568 nm). Condition: 10 C/min. Nitrogen flow: 50 mL/min. The functionalized SWCNTs were dispersed in a 1 wt % SC-D₂O solution for optical measurements.

observation of the SWCNT adducts, the solvent was replaced with 0.05 wt % ammonium deoxycholate (ADC). ADC is reportedly relatively easy to remove using a thermal treatment, as compared to the corresponding sodium salt.⁴² Because functional groups can reportedly be removed through thermal treatment, the PL properties may change due to the removal of

the surfactant. Therefore, SWCNTs-(2ArI₂) was thermally treated at 400 °C for 1 h under a nitrogen flow (SWCNTs-2ArI₂Δ) to evaluate the influence of the thermal treatment on the PL properties (Figure 6). Scanning electron microscopy (SEM) analyses confirmed that the surfactant was adsorbed during the chiral separation process and that they were

removed by the thermal treatment (Figure S16). Additionally, a subsequent thermal treatment of SWCNTs-(2ArI₂Δ) at 400 °C for 20 min under a nitrogen flow containing 5% oxygen was conducted (SWCNTs-(2ArI₂ΔO₂)) according to literature methods.⁴² After these thermal treatments, the E₁₁** PL peak intensity of SWCNTs-(2ArI₂ΔO₂) decreased, whereas the absorption and PL characteristics of SWCNTs-(2ArI₂Δ) were maintained (Figure 6b).

Based on the evaluation of the effect of the thermal treatment on the PL properties, (6,5) SWCNTs-(2ArI₂) was thermally treated for TEM observation after sampling (6,5) SWCNTs-(2ArI₂) on a TEM grid. Before observation, (6,5) SWCNTs-(2ArI₂) was heated at 400 °C for 1 h under vacuum conditions ($\sim 10^{-2}$ Pa) to remove the surfactant. The TEM images revealed that separation and thermal treatment are important for the observation of the SWCNTs. The observation of the SWCNTs was difficult without separation or thermal treatment, likely due to carbonaceous impurities and surfactants (Figure S18). Figure 7a shows a high-resolution TEM image of (6,5) SWCNTs-(2ArI₂) after thermal treatment, where functional groups sparsely attached to the surface of the (6,5) SWCNT can be observed. The magnified TEM image (Figure 7b) of the region where the substituent protrudes from the SWCNT surface agrees well

with the molecular model of 1,4 L₊₊ (6,5) SWCNT-Ph₂ (Figure 7c) and the corresponding simulated TEM image (Figure 7d). Importantly, the molecular models of 1,2 L₊₊ (6,5) SWCNT-Ph₂ and L₋ and L₊ (6,5) SWCNT-Ph₂ (1,2- and 1,4-adducts) viewed from similar angles provided simulated TEM images that were different from the experimental image in Figure 7b, as the two phenyl substituents did not overlap, or the benzene rings were oriented perpendicular to the electron beam direction (Figure S19). These results suggest the formation of 1,4 L₊₊ (6,5) SWCNTs-Ph₂ proposed by a comparison of the PL and theoretical results.

CONCLUSIONS

SWCNTs were reductively arylated in this study using halo- and dihalobenzenes to reveal the effect of halogen atoms on the degree of functionalization and PL characteristics. As with the butyl halide, the degree of functionalization and selectivity of the PL wavelength were dependent on the halogen atom of the phenyl halide. Furthermore, the E₁₁** PL selectivity was significantly improved by reactions using haloiodobenzenes regardless of the type and substitution position of the halogen atom. Separation of the SWCNT adducts based on the chiral index revealed that reductive arylation using the halogen atom effect is an effective method for the selective emergence of a new PL peak from SWCNTs with other chiral indices. It is also effective for the direct observation of addenda on SWCNTs using TEM. These findings are expected to facilitate the use of SWCNTs as NIR light sources in bioimaging, telecommunications, and other related fields.

MATERIALS AND METHODS

The materials were purchased and used without further purification, unless otherwise stated. Tetrahydrofuran (pure, anhydrous) was obtained from Kanto Chemical and purified using a Glass Contour Ultimate solvent purification system (Nikko Hansen Co., Ltd.).

Functionalization of SWCNTs⁴⁴

Naphthalene (300 mg, 2.34 mmol) and sodium (156 mg, 6.80 mmol) were placed in a 200 mL heat-dried three-neck round-bottom flask under argon. Anhydrous tetrahydrofuran (100 mL) was added to the flask, and the mixture was stirred for 1 h. A portion of SWCNTs (10 mg, SG65i, Sigma-Aldrich) in a 200 mL heat-dried three-necked round-bottom flask was placed under argon. Sodium naphthalenide solution was added to the SWCNTs, which were then sonicated for 1 h, followed by the addition of halobenzene derivatives (2.81 or 1.41 mmol) to the mixture. The mixture was sonicated for 30 min and then quenched by the addition of 4 mL of dry ethanol (Kanto Chemical). The resulting black suspension was filtered using a PTFE filter (0.1 μm) and washed with tetrahydrofuran, acetone, methanol, and water by using a dispersion-filtration process. The solid was then dried under a vacuum.

Separation of Functionalized SWCNTs

Chiral index-dependent separation was performed using gel column chromatography.^{28,29} Approximately 4.0 mg of SWCNTs were added to a vial containing 5 mL of aqueous 1.0 wt % sodium cholate (SC) ($\geq 98\%$). The vial was bath-sonicated at 20% output power density for 3 h (Sonics & Materials Inc.; Ultrasonic Processor VCX750). The resulting dispersion was centrifuged at 210,000 g for 1 h in a high-speed centrifuge equipped with an S58A angle rotor (Koki Holdings Co., Ltd.; micro ultracentrifuge CS 100FNX). A 2.0 mL portion of aqueous 2.0 wt % SDS ($\geq 97\%$) was added to 2.0 mL of the supernatant solution before the high-performance column chromatography (HPLC) separation. The helicity sorting and optical resolution of the SWCNTs were achieved via HPLC using a JASCO ChromNAV system equipped with a JASCO LC-Net II

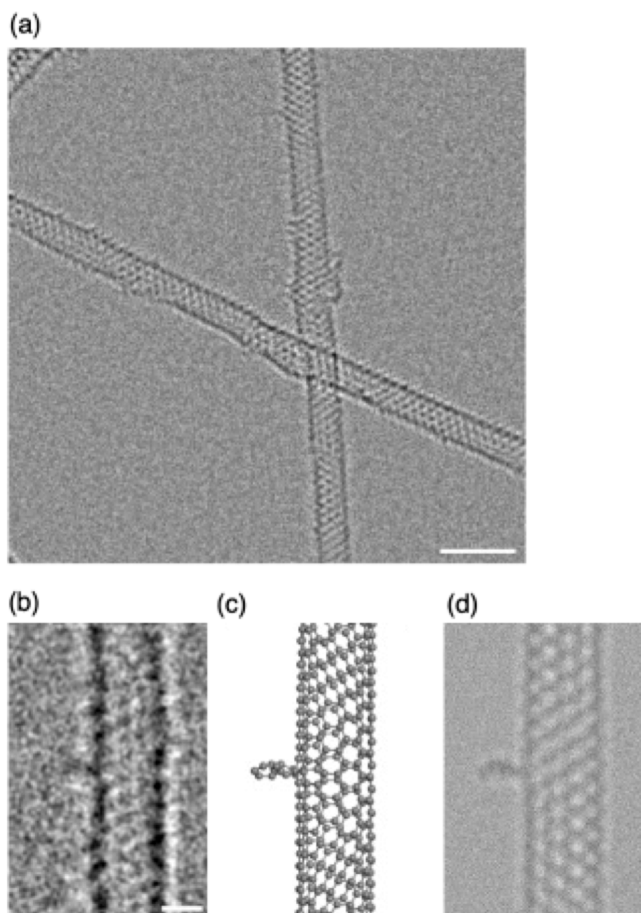


Figure 7. TEM characterization of (6,5) SWCNTs-(2ArI₂). (a) TEM image of (6,5) SWCNTs-(2ArI₂) after thermal treatment to remove surfactants. Scale bar: 2 nm. (b) High-magnification TEM image. Scale bar: 5 Å. (c) Model of 1,4 L₊₊ (6,5) SWCNT-Ph₂ presented as an atomic-number-correlated molecular model.⁴³ (d) Corresponding TEM simulation image.

interface, a JASCO PU-2089i gradient inert pump, a JASCO MD-4010 photodiode array detector, a CO-4060 column oven (23 °C), and a column ($\phi 10 \times 200$ mm) filled with the gel (Sephacryl S-200, Cytiva). The flow rate was 2.0 mL min⁻¹, and the sample (SWCNT dispersion) injection volume was 3 mL. The eluent was an aqueous solution containing 0.5 wt % SC + 0.5 wt % SDS + X wt % DOC (>96%). The concentration of DOC (X) increased from 0 to 1. Fractions were collected every 5 mL using a fraction collector.

Optical Measurements

Optical absorption spectra were recorded using a spectrophotometer (V-670; JASCO Corp.) in a quartz cell with a path length of 10 mm. Raman spectra ($\lambda_{\text{ex}} = 561$ nm) were recorded using a spectrophotometer (LabRAM HR-800; HORIBA Ltd.). These spectra were normalized relative to the G-band. The NIR fluorescence intensity as a function of the excitation and emission wavelengths of the dispersed SWCNTs was obtained using a spectrophotometer equipped with a 450 W lamp and a Symphony-II CCD detector (Nanolog; HORIBA Ltd.). The excitation and emission spectral slit widths were both set to 10 nm. The PL intensity was normalized by the integration time. PL spectra were recorded at a 90° angle relative to the excitation light, unless otherwise stated. The CD spectra of the separated samples were measured at 20 °C by using a CD spectropolarimeter (J-820; JASCO Corp.).

FE-SEM Observation

SEM images were measured on a Hitachi FE-SEM SU-8020 SEM. Carbon double-tape was used to attach the sample to the stub holder.

TEM Observation

TEM observation was carried out on an aberration-corrected TEM instrument (FEI Titan Cubed) at an acceleration voltage of 80 kV under 4×10^{-6} Pa in the specimen column using a monochromator for the incident electron beam ($\Delta E = 0.15$ eV). Images were captured and processed on a CMOS camera (Gatan OneView, D mode, 4096 \times 4096 pixels) operated in binning 2 mode. The images were recorded at under-focus conditions (defocus value: ca. -8 nm) at an electron dose rate of ca. 1×10^6 e⁻ nm⁻² s⁻¹, and the exposure time was set to 1.0 s. Since suspended (6,5) SWCNTs were frequently vibrated under electron beam irradiation, a series of images was continuously recorded at a frame rate of 25 frames per second at an electron dose rate of ca. 1×10^6 e⁻ nm⁻² s⁻¹, and 25 consecutive images in the video were superimposed after translational motion correction to obtain a higher signal-to-noise-ratio image, which was then filtered using a bandpass filter (filtering structures smaller than 3 pixels and larger than 40 pixels, tolerance of direction: 5%). TEM image simulation was performed by using a multislice procedure implemented in Elbis software.⁴⁵

Computational Details

One unit cell of (6,5), (7,3), and (8,3) SWCNTs was adopted as the computational model for the functionalized SWCNTs. The dangling bonds at the terminals were passivated with hydrogen atoms or a mixture of hydrogen atoms and two methylene groups to eliminate midgap trap states. The geometry optimization was performed using the B3LYP functional combined with the 6-31G* basis set.^{30–34} TD-DFT calculations were carried out at the B3LYP/3-21G level of theory. All DFT calculations were performed using the Gaussian 09 software suite, version E.01.³⁵

■ ASSOCIATED CONTENT

Supporting Information

The Supporting Information is available free of charge at <https://pubs.acs.org/doi/10.1021/acsnanoscienceau.5c00152>.

Raman, absorption, CD, PL, and XPS spectra and SEM and TEM images of functionalized SWCNTs; HOMO and LUMO distributions in (6,5) SWCNT-C₆H₄; calculated relative energies, transition energies, and oscillator strength of functionalized SWCNTs; and

spin density of the Ph-(6,5) SWCNT radical and CH₃(CH₂)₃-(6,5) SWCNT radical (PDF)

■ AUTHOR INFORMATION

Corresponding Authors

Yutaka Maeda – Department of Chemistry, Tokyo Gakugei University, Tokyo 184-8501, Japan; orcid.org/0000-0003-0502-5621; Email: ymaeda@u-gakugei.ac.jp

Masahiro Ehara – Research Center for Computational Science, Institute for Molecular Science, Okazaki 444-8585, Japan; orcid.org/0000-0002-2185-0077; Email: ehara@ims.ac.jp

Koji Harano – Center for Basic Research on Materials, National Institute for Materials Science, Tsukuba 305-0044, Japan; Research Center for Autonomous Systems Materialogy (ASMat), Institute of Integrated Research, Institute of Science Tokyo, Yokohama 226-8501, Japan; orcid.org/0000-0001-6800-8023; Email: HARANO.Koji@nims.go.jp

Authors

Atsushi Suwa – Department of Chemistry, Tokyo Gakugei University, Tokyo 184-8501, Japan

Kentaro Kawada – Department of Chemistry, Tokyo Gakugei University, Tokyo 184-8501, Japan

Pei Zhao – Research Center for Computational Science, Institute for Molecular Science, Okazaki 444-8585, Japan; orcid.org/0000-0002-8088-6141

Yasuhiro Suzuki – Department of Chemistry, Tokyo Gakugei University, Tokyo 184-8501, Japan

Yui Iguchi – Department of Chemistry, Tokyo Gakugei University, Tokyo 184-8501, Japan

Yasunari Taki – Department of Chemistry, Tokyo Gakugei University, Tokyo 184-8501, Japan

Yui Konno – Department of Chemistry, Tokyo Gakugei University, Tokyo 184-8501, Japan

Michio Yamada – Department of Chemistry, Tokyo Gakugei University, Tokyo 184-8501, Japan; orcid.org/0000-0002-6715-4202

Hitoshi Kasai – Institute of Multidisciplinary Research for Advanced Materials (IMRAM), Tohoku University, Sendai 980-8577, Japan; orcid.org/0000-0001-9399-0506

Koji Kimoto – Center for Basic Research on Materials, National Institute for Materials Science, Tsukuba 305-0044, Japan; orcid.org/0000-0002-3927-0492

Complete contact information is available at:

<https://pubs.acs.org/doi/10.1021/acsnanoscienceau.5c00152>

Author Contributions

Y.M. conceived the idea of this study and designed the experiments. Nanotube functionalization, separation, optical characterization, and data analysis were performed by A.S., K.K., Y.T., Y.I., Y.S., Y.K., and M.Y. XPS analysis was conducted by H.K. Theoretical calculations were designed and performed by P.Z. and M.E. K.H. and K.K. conducted TEM observation. All authors contributed to the analysis and interpretation of results. Y.M., M.E., and K.H. wrote the manuscript with the assistance of all coauthors.

Notes

The authors declare no competing financial interest.

■ ACKNOWLEDGMENTS

This study was supported by JSPS KAKENHI Grant-in-Aid for Scientific Research (B)(JP21H01759, JP20H02210, JP20H02718, JP17H02735) and Transformative Research Areas (A) (JP22H05133 and JP23H04874). This study was performed under the Cooperative Research Programme of the “Network Joint Research Centre for Materials and Devices”. I wish to thank Professor Koseki Yoshitaka, Prefectural University of Hiroshima, for supporting XPS measurements.

■ ABBREVIATIONS

SWCNT, single-walled carbon nanotube; NIR, near-infrared; PL, photoluminescence; XPS, X-ray photoelectron spectroscopy; TEM, transmission electron microscopy; ADC, ammonium deoxycholate; SEM, scanning electron microscopy

■ REFERENCES

- (1) Iijima, S.; Ichihashi, T. Single-shell Carbon Nanotubes of 1-nm Diameter. *Nature* **1993**, *363*, 603–605.
- (2) Bethune, D. S.; Kiang, C. H.; de Vries, M. S.; Gorman, G.; Savoy, R.; Vazquez, J.; Beyers, R. Cobalt-catalysed Growth of Carbon Nanotubes with Single-atomic-layer Walls. *Nature* **1993**, *363*, 605–607.
- (3) Tasis, D.; Tagmatarchis, N.; Bianco, A.; Prato, M. Chemistry of Carbon Nanotubes. *Chem. Rev.* **2006**, *106*, 1105–1136.
- (4) Karousis, N.; Tagmatarchis, N.; Tasis, D. Current Progress on the Chemical Modification of Carbon Nanotubes. *Chem. Rev.* **2010**, *110*, 5366–5397.
- (5) Saito, R.; Fujita, M.; Dresselhaus, G.; Dresselhaus, M. S. Electronic Structure of Chiral Graphene Tubules. *Appl. Phys. Lett.* **1992**, *60*, 2204–2206.
- (6) Ghosh, S.; Bachelo, S. M.; Simonette, R. A.; Beckingham, K. M.; Weisman, R. B. Oxygen Doping Modifies Near-infrared Band Gaps in Fluorescent Single-walled Carbon Nanotubes. *Science* **2010**, *330*, 1656–1659.
- (7) Brozena, A. H.; Kim, M.; Powell, L. R.; Wang, Y. H. Controlling the Optical Properties of Carbon Nanotubes with Organic Colour-centre Quantum Defects. *Nat. Rev. Chem.* **2019**, *3*, 375–392.
- (8) Gifford, B. J.; Kilina, S.; Htoon, H.; Doorn, S. K.; Tretiak, S. Controlling Defect-state Photophysics in Covalently Functionalized Single-walled Carbon Nanotubes. *Acc. Chem. Res.* **2020**, *53*, 1791–1801.
- (9) Shiraki, T.; Miyauchi, Y.; Matsuda, K.; Nakashima, N. Carbon Nanotube Photoluminescence Modulation by Local Chemical and Supramolecular Chemical Functionalization. *Acc. Chem. Res.* **2020**, *53*, 1846–1859.
- (10) Janas, D. Perfectly imperfect: A Review of Chemical Tools for Exciton Engineering in Single-walled Carbon Nanotubes. *Mater. Horiz.* **2020**, *7*, 2860–2881.
- (11) Zaumseil, J. Luminescent Defects in Single-Walled Carbon Nanotubes for Applications. *Adv. Opt. Mater.* **2022**, *10*, 2101576.
- (12) Maeda, Y.; Zhao, P.; Ehara, M. Recent Progress in Controlling the Photoluminescence Properties of Single-walled Carbon Nanotubes by Oxidation and Alkylation. *Chem. Commun.* **2023**, *59*, 14497–14508.
- (13) Piao, Y.; Meany, B.; Powell, L. R.; Valley, N.; Kwon, H.; Schatz, G. C.; Wang, Y. Brightening of Carbon Nanotube Photoluminescence through the Incorporation of sp^3 Defects. *Nat. Chem.* **2013**, *5*, 840–845.
- (14) Kilina, S.; Ramirez, J.; Tretiak, S. Brightening of the Lowest Exciton in Carbon Nanotubes via Chemical Functionalization. *Nano Lett.* **2012**, *12*, 2306–2312.
- (15) Ma, X.; Adamska, L.; Yamaguchi, H.; Yalcin, S. E.; Tretiak, S.; Doorn, S. K.; Htoon, H. Electronic Structure and Chemical Nature of Oxygen Dopant States in Carbon Nanotubes. *ACS Nano* **2014**, *8*, 10782–10789.
- (16) He, X.; Gifford, B. J.; Hartmann, N. F.; Ihly, R.; Ma, X.; Kilina, S. V.; Luo, Y.; Shayan, K.; Strauf, S.; Blackburn, J. L.; et al. Low-Temperature Single Carbon Nanotube Spectroscopy of sp^3 Quantum Defects. *ACS Nano* **2017**, *11*, 10785–10796.
- (17) Zhao, P.; Maeda, Y.; Ehara, M. Theoretical Insight into Configurational Selectivity of Functionalized Single-Walled Carbon Nanotubes Based on the Clar Sextet Theory. *J. Phys. Chem. C* **2019**, *123*, 18629–18637.
- (18) Wang, P.; Fortner, J.; Luo, H.; Klos, J.; Wu, X.; Qu, H.; Chen, F.; Li, Y.; Wang, Y. Quantum Defects: What Pairs with the Aryl Group When Bonding to the sp^2 Carbon Lattice of Single-Wall Carbon Nanotubes? *J. Am. Chem. Soc.* **2022**, *144*, 13234–13241.
- (19) Yu, B.; Naka, S.; Aoki, H.; Kato, K.; Yamashita, D.; Fujii, S.; Kato, Y. K.; Fujigaya, T.; Shiraki, T. *ortho*-Substituted Aryldiazonium Design for the Defect Configuration-Controlled Photoluminescent Functionalization of Chiral Single-Walled Carbon Nanotubes. *ACS Nano* **2022**, *16*, 21452–21461.
- (20) Maeda, Y.; Iguchi, Y.; Zhao, P.; Suwa, A.; Taki, Y.; Kawada, K.; Yamada, M.; Ehara, M.; Kako, M. Switching Photoluminescence Wavelength of Arylated Single-walled Carbon Nanotubes by Utilizing Steric Hindrance in Reductive Arylation. *Chem.—Eur. J.* **2025**, *31*, No. e202404529.
- (21) Maeda, Y.; Takehana, Y.; Yamada, M.; Suzuki, M.; Murakami, T. Control of the Photoluminescence Properties of Single-walled Carbon Nanotubes by Alkylation and Subsequent Thermal Treatment. *Chem. Commun.* **2015**, *51*, 13462–13465.
- (22) Maeda, Y.; Morooka, R.; Zhao, P.; Uchida, D.; Konno, Y.; Yamada, M.; Ehara, M. Controlling Near-Infrared Photoluminescence Properties of Single-Walled Carbon Nanotubes by Substituent Effect in Stepwise Chemical Functionalization. *J. Phys. Chem. C* **2023**, *127*, 2360–2370.
- (23) Dzienia, A.; Taborowska, P.; Kubica-Cypek, P.; Janas, D. Programming Optical Properties of Single-walled Carbon Nanotubes with Benzoyl Peroxide Derivatives of Tailored Chemical Characteristics. *Nanoscale Horiz.* **2025**, *12*, 9040–9056.
- (24) Pause, L.; Robert, M.; Savéant, J.-M. Can Single-Electron Transfer Break an Aromatic Carbon–Heteroatom Bond in One Step? A Novel Example of Transition between Stepwise and Concerted Mechanisms in the Reduction of Aromatic Iodides. *J. Am. Chem. Soc.* **1999**, *121*, 7158–7159.
- (25) Maeda, Y.; Suzuki, Y.; Konno, Y.; Zhao, P.; Kikuchi, N.; Yamada, M.; Mitsuishi, M.; Dao, A. T. N.; Kasai, H.; Ehara, M. Selective Emergence of Photoluminescence at Telecommunication Wavelengths from Cyclic Perfluoroalkylated Carbon Nanotubes. *Chem. Commun.* **2023**, *6*, 159.
- (26) Kwon, H.; Furmanchuk, A.; Kim, M.; Meany, B.; Guo, Y.; Schatz, G. C.; Wang, Y. Molecularly Tunable Fluorescent Quantum Defects. *J. Am. Chem. Soc.* **2016**, *138*, 6878–6885.
- (27) Gifford, B. J.; He, X.; Kim, M.; Kwon, H.; Saha, A.; Sifain, A. E.; Wang, Y.; Htoon, H.; Kilina, S.; Doorn, S. K.; et al. Optical Effects of Divalent Functionalization of Carbon Nanotubes. *Chem. Mater.* **2019**, *31*, 6950–6961.
- (28) Yomogida, Y.; Tanaka, T.; Zhang, M.; Yudasaka, M.; Wei, X.; Kataura, H. Industrial-scale Separation of High-purity Single-chirality Single-wall Carbon Nanotubes for Biological Imaging. *Nat. Commun.* **2016**, *7*, 12056.
- (29) Maeda, Y.; Konno, Y.; Yamada, M. Helicity Sorting and Optical Resolution of Functionalized Single-Walled Carbon Nanotubes and Their Optical Properties. *J. Phys. Chem. C* **2020**, *124*, 21886–21894.
- (30) Becke, A. D. Density-functional Thermochemistry. III. The Role of Exact Exchange. *J. Chem. Phys.* **1993**, *98*, 5648–5652.
- (31) Lee, C.; Yang, W.; Parr, R. G. Development of the Colle-Salvetti Correlation-energy Formula into a Functional of the Electron Density. *Phys. Rev. B* **1988**, *37*, 785–789.
- (32) Stephens, P. J.; Devlin, F. J.; Chabalowski, C. F.; Frisch, M. J. Ab Initio Calculation of Vibrational Absorption and Circular Dichroism Spectra Using Density Functional Force Fields. *J. Phys. Chem.* **1994**, *98*, 11623–11627.

- (33) Hariharan, P. C.; Pople, J. A. The Influence of Polarization Functions on Molecular Orbital Hydrogenation Energies. *Theor. Chim. Acta* **1973**, *28*, 213–222.
- (34) Hehre, W. J.; Ditchfield, R.; Pople, J. A. Self-Consistent Molecular Orbital Methods. XII. Further Extensions of Gaussian-Type Basis Sets for Use in Molecular Orbital Studies of Organic Molecules. *J. Chem. Phys.* **1972**, *56*, 2257–2261.
- (35) Frisch, M. J.; Trucks, G. W.; Schlegel, H. B.; Scuseria, G. E.; Robb, M. A.; Cheeseman, J. R.; Scalmani, G.; Barone, V.; Mennucci, B.; Pettersson, G. A.; et al. *Gaussian 09*, Revision E.01; Gaussian, Inc.: Wallingford, CT, 2013.
- (36) Maeda, Y.; Murakoshi, H.; Tambo, H.; Zhao, P.; Kuroda, K.; Yamada, M.; Zhao, X.; Nagase, S.; Ehara, M. Thermodynamic Control of Quantum Defects on Single-walled Carbon Nanotubes. *Chem. Commun.* **2019**, *55*, 13757–13760.
- (37) Maeda, Y.; Morooka, R.; Zhao, P.; Yamada, M.; Ehara, M. Control of Functionalized Single-walled Carbon Nanotube Photoluminescence via Competition between Thermal Rearrangement and Elimination. *Chem. Commun.* **2023**, *59*, 11648–11651.
- (38) M'Halla, F.; Pinson, J.; Savéant, J. M. The Solvent as H-atom Donor in Organic Electrochemical Reactions. Reduction of Aromatic Halides. *J. Am. Chem. Soc.* **1980**, *102*, 4120–4127.
- (39) Capaldo, L.; Ravelli, D. Hydrogen Atom Transfer (HAT): A Versatile Strategy for Substrate Activation in Photocatalyzed Organic Synthesis. *Eur. J. Org. Chem.* **2017**, *15*, 2056–2071.
- (40) Smith, B. W.; Monthieux, M.; Luzzi, D. E. Encapsulated C₆₀ in Carbon Nanotubes. *Nature* **1998**, *396*, 323–324.
- (41) Umeyama, T.; Baek, J.; Sato, Y.; Suenaga, K.; Abou-Chahine, F.; Tkachenko, N. V.; Lemmetyinen, H.; Imahori, H. Molecular Interactions on Single-walled Carbon Nanotubes Revealed by High-resolution Transmission Microscopy. *Nat. Commun.* **2015**, *6*, 7732.
- (42) Zhang, C.; Wang, P.; Barnes, B.; Fortner, J.; Wang, Y. Cleanly Removable Surfactant for Carbon Nanotubes. *Chem. Mater.* **2021**, *33*, 4551–4557.
- (43) Xing, J.; Takeuchi, K.; Kamei, K.; Nakamuro, T.; Harano, K.; Nakamura, E. Atomic-number (Z)-correlated Atomic Sizes for Deciphering Electron Microscopic Molecular Images. *Proc. Natl. Acad. Sci. U.S.A.* **2022**, *119*, No. e2114432119.
- (44) Maeda, Y.; Minami, S.; Takehana, Y.; Dang, J. S.; Aota, S.; Matsuda, K.; Miyauchi, Y.; Yamada, M.; Suzuki, M.; Zhao, R. S.; et al. Tuning of the Photoluminescence and Up-conversion Photoluminescence Properties of Single-walled Carbon Nanotubes by Chemical Functionalization. *Nanoscale* **2016**, *8*, 16916–16921.
- (45) Hosokawa, F.; Shinkawa, T.; Arai, Y.; Sannomiya, T. Benchmark Test of Accelerated Multi-slice Simulation by GPGPU. *Ultramicroscopy* **2015**, *158*, 56–64.



CAS BIOFINDER DISCOVERY PLATFORM™

PRECISION DATA FOR FASTER DRUG DISCOVERY

CAS BioFinder helps you identify
targets, biomarkers, and pathways

Unlock insights

CAS
A division of the
American Chemical Society